A LETTERS JOURNAL EXPLORING
THE FRONTIERS OF PHYSICS

October 2023

EPL, **144** (2023) 26002
doi: 10.1209/0295-5075/ad0573

www.epljournal.org

Enhanced nucleation of bimodal molecular weight distribution polymers: A molecular dynamics study

ZENGQIANG ZHAI, JULIEN MORTHOMAS[(a)], CLAUDIO FUSCO, MICHEL PEREZ and OLIVIER LAME

Univ. de Lyon, INSA Lyon, MATEIS, UMR CNRS 5510 - 69621 Villeurbanne, France

received 4 July 2023; accepted in final form 20 October 2023

Abstract – We perform coarse-grained molecular dynamics (CGMD) simulations to study the homogeneous nucleation of bimodal and unimodal molecular weight distribution polymers with equivalent average molecular weight. First, a statistical method is proposed to determine the critical nuclei and thus calculate the free energy barrier of nucleation. From the temperature dependence of diffusion coefficient, we also determine the activation energy of diffusion. Then we calculate the nucleation rate and find that it is consistent with the classical nucleation theory for homogeneous nucleation in semi-crystalline polymers. Compared with unimodal system, the bimodal system exhibits lower interfacial free energy and consequently lower free energy barrier for nucleation, while the two systems have similar activation energy for diffusion. This suggests that the promoted nucleation rate of bimodal molecular weight distribution polymer is a result of the reduction of interfacial free energy, which is eventually a consequence of chain-folding nucleation of long chain component.

Polymer crystallization consists of two stages: homogeneous nucleation and crystal growth. Extensive investigations [1–5] have been done on the second stage using both experimental and simulation techniques. The nucleation rate strongly depends on the free energy barrier of a critical nucleus, governed by a competition between the loss in free energy to create the crystalline nuclei, and the gain in the interfacial free energy of the crystal-melt interface. Before the nucleation stage, an induction period of a precrystallization assisted by spinodal phase separation can be observed [6]. Experimental measurements of polymer crystal-melt surface tension are challenging, and homogeneous nucleation experiments are quite difficult to carry out. Only a few experiments [7–9] have been performed in pure droplets with an emulsion of molten polymer, where homogeneous crystallization is monitored by *in situ* microscopy or by wide-angle X-ray scattering. Surface tensions then have been obtained by fitting classical nucleation theory (CNT) to experimental results [9–11].

Analytical theory and molecular simulation provide an alternative way for obtaining the polymer interfacial free energies. Self-consistent field theory [12] has been used to analytically obtain interfacial free energy from the equilibrium crystal-melt interface of polyethylene, by assuming the chain end surface to be a grafted brush of chain folds in a self-consistent pressure field. Wedekind *et al.* [13] and other researchers [14–16] calculated the size of critical nuclei using a mean first-passage time analysis by tracing the growth of nuclei and assumed in this case the validity of classical nucleation theory without testing the theory or the assumptions.

Only a few works [3,17–19] have addressed the nucleation of bimodal polymers, which remains poorly understood compared to unimodal polymers. Qi *et al.* [18] showed that the free energy barrier, as well as the critical nucleus is sensitive to polydispersity. It was also claimed that blending long chains to a short chain melt could promote the nucleation rate [3,20], and this effect was attributed to long chains. However, the average molecular weight was also promoted with blending of long chains. In ref. [19], a self-seeding method is used to study the nucleation and growth of branched bidisperse semi-crystalline polymers in order to improve the crystallization morphology of the resulting structure.

In this work, coarse-grained molecular dynamics (CGMD) simulations have been performed to investigate the homogeneous and isothermal nucleation of bimodal and unimodal molecular weight distribution (MWD) polymers with equivalent average molecular weight. A statistical approach has been applied for computing the size of critical nuclei from which both the interfacial free energy and the free energy barrier for nucleation can be deduced.

[(a)] E-mail: julien.morthomas@insa-lyon.fr (corresponding author)

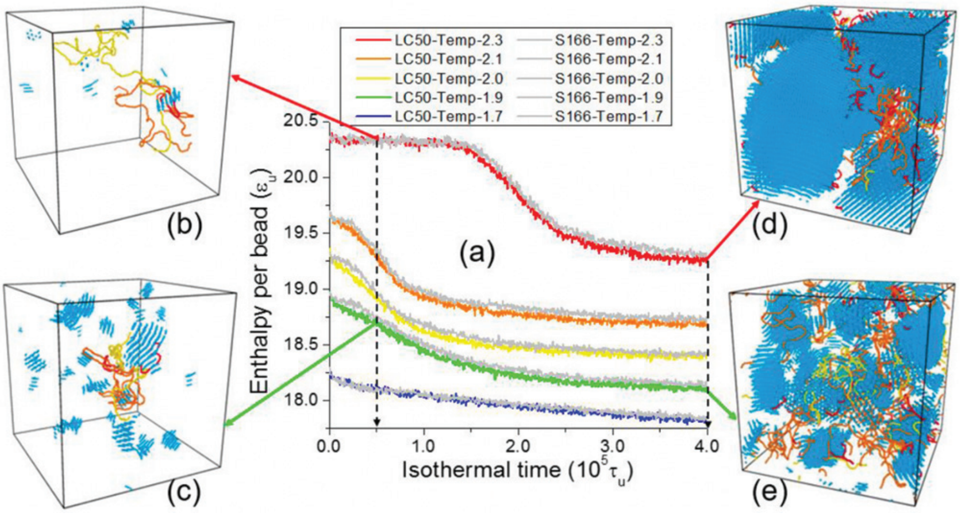

Fig. 1: (a) Thermograms of isothermal treatment of uni- ("S" for single in the legend) and bimodal ("LC" for the presence of long chains) systems at constant temperatures 2.3, 2.1, 1.9 and $T = 1.7\epsilon_u/k_B$ respectively for a period of $4.0 \times 10^5\tau_u$. (b) and (c): snapshots of bimodal system after $0.5 \times 10^5\tau_u$ of crystallization with isothermal temperatures of 2.3 and $1.9\epsilon_u/k_B$, respectively, and (d) and (e) at the end of isothermal treatment. Colors in snapshots (b)–(e): blue represents the crystal phase, red loop segments, orange tie segments, and yellow cilia segments.

After obtaining the activation energy of diffusion, the nucleation rate has been evaluated with classical nucleation theory and compared to the one directly calculated from CGMD simulations.

The CNT method has been widely used to describe homogeneous nucleation. In semi-crystalline polymers, two types of crystal interfaces with the melt are formed: chain-end surface and side surface. A cylinder model is often assumed to describe the shape of nuclei. The free energy of formation of a cylindrical crystal nucleus is given by $\Delta G = 2\pi r^2\sigma_e + 2\pi rl\sigma_s - \pi r^2 l\Delta G_v$, where σ_s and σ_e are the interfacial free energies for respectively the side and end surfaces of a cylindrical nucleus of radius r and length l, and which may depend on the temperature, and ΔG_v is the Gibbs free energy difference per unit volume between the crystal and melt phases. For deep supercooling, an approximation for ΔG_v is

$$\Delta G_v \approx \rho_n \Delta H_f \frac{T\left(T_m - T\right)}{T_m^2}, \tag{1}$$

where ρ_n is the crystal density, ΔH_f is the melting heat at the thermodynamic equilibrium melting temperature T_m [21]. Maximizing ΔG with respect to r and l gives the free energy barrier ΔG^*,

$$\Delta G^* = 8\pi \frac{\sigma_s^2\left(T\right)\sigma_e\left(T\right)}{\Delta G_v{}^2}, \tag{2}$$

and the critical nucleus size n^*,

$$n^* = 16\pi\rho_n \frac{\sigma_s^2\left(T\right)\sigma_e\left(T\right)}{\Delta G_v{}^3}. \tag{3}$$

According to CNT, Kampmann and Wagner [21] introduced the nucleation rate at steady state, leading to the following expression:

$$\left.\frac{\mathrm{d}N}{\mathrm{d}t}\right|_{nuclei} = Ae^{-\frac{E_d}{k_B T}} e^{-\frac{\Delta G^*}{k_B T}}, \tag{4}$$

where $\mathrm{d}N/\mathrm{d}t|_{nuclei}$ is the nucleation rate in the number of nuclei formed per unit volume and per unit time, E_d the activation energy for chain mobility and A a constant prefactor, assuming a temperature-independent Zeldovich factor.

In our semicrystalline CGMD model, polymer chains consist of a succession of "beads" representing a few structural units. It is based on two potentials: a finite-extensible non-linear elastic (FENE) potential which models intra-chain interactions of bonded beads, and a Lennard-Jones (LJ) potential which models weak interactions of non-bonded beads. Energy, length, and time units are given by ε_u, σ_u and τ_u, respectively (with $\tau_u = \sqrt{m_u\sigma_u^2/\epsilon_u}$, where m_u is the mass unit). The potential parameters were optimized so that the polymer chains tend to align and form thermally stable crystallites (for the details please refer to our previous publications [16,22–24]). The bimodal system consists of 100 long chains of 500 beads and 500 short chains of 100 beads, corresponding to 50% of weight fraction of long chain content and an average molecular weight of $166.7m_u$. We have also prepared a unimodal system consisting of 600 chains of 166 beads, which has the same molecular weight as the bimodal system. The two systems have been relaxed for a sufficiently long time of $5.0 \times 10^5\tau_u$ at $T = 4\epsilon_u/k_B$, above the thermodynamic equilibrium melting temperature $T_m = 3.1\varepsilon_u/k_B$, calculated in a previous work [23], until reaching a state of thermodynamical equilibrium. Then the systems are submitted to a fast-cooling process (cooling rate: $10^{-5}\epsilon_u/k_B/\tau_u$) to the target temperatures 2.5, 2.3, 2.2, 2.1, 2.0, 1.9, 1.7 and $1.5\epsilon_u/k_B$, respectively. Afterwards, the temperatures of the systems are maintained constant for the isothermal treatment, until the crystallization of each system saturates. At $2.5\epsilon_u/k_B$, no crystallization was observed. Figure 1 shows the enthalpies as a function of isothermal time just after the cooling. We can see that only at temperature $2.3\epsilon_u/k_B$ the enthalpy shows an incubation time and then starts to decrease indicating the onset of crystallization, while the crystallization occurs almost instantly at lower temperatures. At $4.0 \times 10^5\tau_u$ the enthalpy of all the systems reaches a plateau, indicating maximum crystallinities. Figure 1(b)–(e) provides snapshots at the early stage and at the end of crystallization for bimodal system at temperatures 2.3 and $1.9\epsilon_u/k_B$, respectively. Lamellae-like structures with tapered edge have been obtained at high temperature of $2.3\epsilon_u/k_B$, whereas numerous small crystallites are detected at lower temperature of $1.9\epsilon_u/k_B$. In fig. 1(b), we can observe crystal nucleation events with no evidence of a phase separation process within the amorphous phase, as in ref. [6].

In the process of isothermal treatment, statistical calculation of the critical size of nucleus n^* is based on the increase and decrease of the nucleus size. According to CNT, the critical size of a nucleus is a point of unstable equilibrium, with equal probability for a nucleus to either grow or shrink. In our statistical approach, we calculate the sizes of all the nuclei growing and shrinking in the process of isothermal treatment. Assume that a nucleus at time t contains n_t beads, and a nucleus at time $t + \Delta t$ contains $n_{t+\Delta t}$ beads. If these two nuclei have more than $n_t/2$ common beads, they are considered as the same nucleus. If the same nucleus is not found at $t + \Delta t$, it means that the size of this nucleus $n_{t+\Delta t}$ shrinks to zero. Thus, all the nuclei at time t are compared to those at time $t + \Delta t$ and all the nuclei growing and shrinking are detected. If $n_t \leq n_{t+\Delta t}$, it means a growing event occurs, and the number of growing events $G(n_t)$ is increased by 1; otherwise, the number of shrinking events $S(n_t)$ is increased by 1. After obtaining a large statistic, the growing probability of a nucleus, $P(n)$ with size n will be

$$P(n) = \frac{G(n)}{G(n) + S(n)}. \tag{5}$$

In this way, the probability of growing $P(n)$ as a function of nucleus size n will be obtained. The critical nucleus size is deduced for a size n^* such that $P(n^*) = 50\%$. The configurations are taken every $\Delta t = 100\tau_u$. The inset in fig. 2 shows the probability of growing of a nucleus for the bimodal system at temperature $2.1\epsilon_u/k_B$. In this case the critical nucleus size is 135 beads. Using the mean first passage method in our previous work [16], the critical size of a nucleus in the same case was determined to be 129. The difference is within 5%, which verifies the validity of our statistical approach. In this way, we have determined the critical nucleus size of bimodal and unimodal systems at several temperatures, see fig. 2.

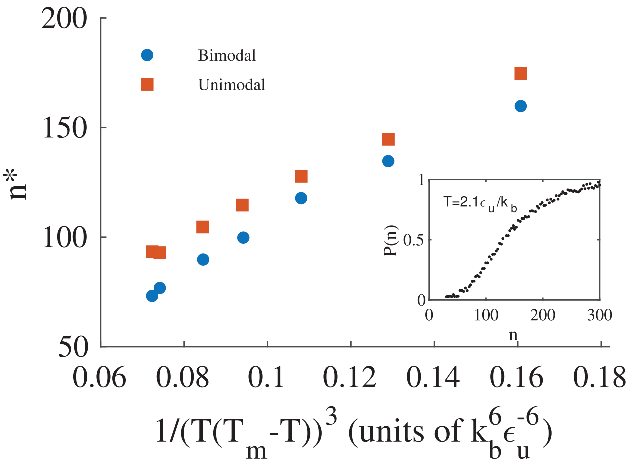

Fig. 2: Critical nucleus size n^* of bimodal (blue circles) and unimodal (red squares) system as a function of $1/(T(T_m - T))^3$. Inset: probability of nucleus growing $P(n)$ as a function of nucleus size A of the bimodal system at temperature $T = 2.1\epsilon_u/k_B$.

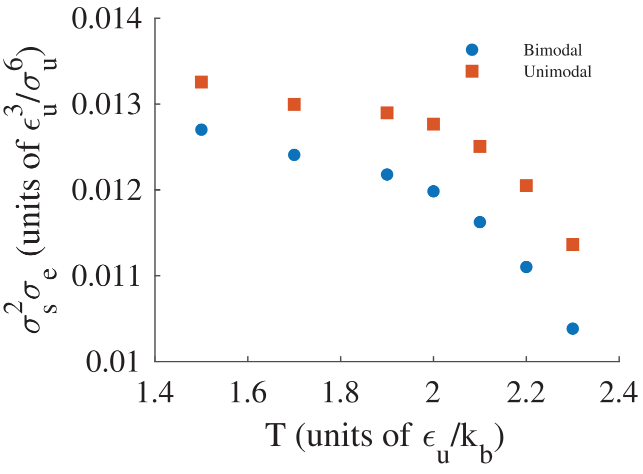

Fig. 3: Interfacial free energy ($\sigma_s^2\sigma_e$) as a function of temperature.

The interfacial free energy $\sigma_s^2\sigma_e$ can then be evaluated as a function of temperature with eqs. (1) and (3). For this purpose, we use the value of the melting heat ΔH_f that we have determined in a previous work, (see table II in [23]): $\Delta H_f = 1.9\varepsilon_u$ and $\rho_n = 0.30\sigma_u^{-3}$. As observed in fig. 3, the interfacial free energy of the bimodal system is lower than that of unimodal system, but both decrease with temperature, displaying a more pronounced drop when the temperature increases up to $2.1\epsilon_u/k_B$. This decreasing trend is in qualitative agreement with experimental observation in a polymer melt [25], suggesting that CNT yields a physically plausible trend. The drop of the interfacial free energy with temperature can be explained by the significant entropy loss arising from the overcrowded surface. In ref. [16], we showed that the intramolecular chain-folding mode occurs preferentially for bidisperse systems with a larger fraction of long chains, while it is almost

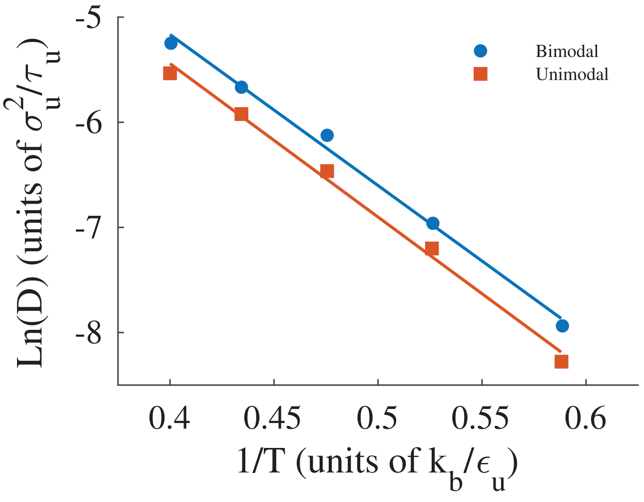

Fig. 4: Diffusion coefficient of bimodal (blue circles) and unimodal (red squares) system as a function of $1/T$. Lines correspond to linear fit to find the activation energy E_d.

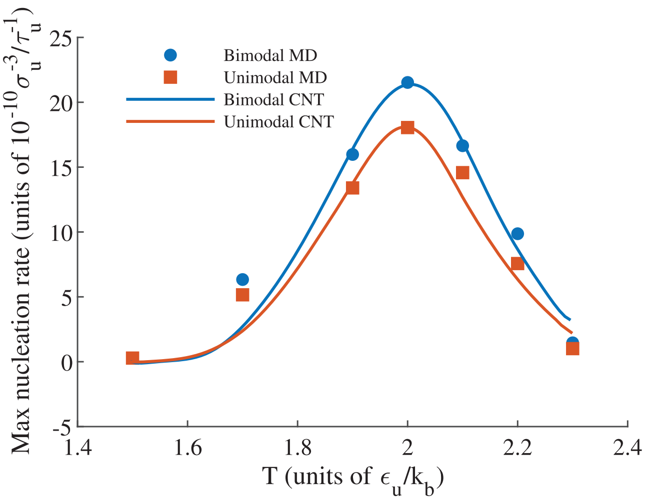

Fig. 5: Temperature dependence of the nucleation rate. The points, blue circles, and red squares for bimodal and unimodal systems respectively, are directly calculated by molecular dynamics simulation. Lines come from CNT.

absent in the unimodal system. We found a correlation between the decreasing behavior of the interfacial free energy and the increase of the fraction of tight loops with the weight fraction of long chains. Thus, we can infer that the enhancement of nucleation is linked to the intramolecular chain folding. Having obtained the interfacial free energy $\sigma_s^2\sigma_e$, the free energy barrier ΔG^* can then be calculated by eqs. (1) and (2).

Next, in order to determine the activation energy of diffusion, we calculate the mean square displacement (MSD) of the centers of mass of the chains, $\langle r^2(t)\rangle$, on a sufficiently long time (more than $30000\tau_u$), as described in Harmandaris *et al.* [26], for the bimodal and unimodal systems at several temperatures in the range 1.7–$2.5\epsilon_u/k_B$. According to Fick's law $\langle r^2(t)\rangle = 6Dt^v$ [27], where here $v = 1$, we can evaluate the self-diffusion coefficient D and thus, the activation energy E_d through the Arrhenius law, $D = D_0 \exp(-E_d/k_BT)$ (see fig. 4). We find $E_d = 14.28\varepsilon_u$ and $E_d = 14.14\varepsilon_u$ for bimodal and unimodal system, respectively. This suggests that E_d is not sensitive to bimodality if the average molecular weight is the same, and the bimodality dependence of diffusion coefficient is mainly controlled by the parameter D_0. However, the diffusion coefficient of bimodal system is larger than that of unimodal system, and the difference increases with temperature. We believe that the diffusion coefficient of the bimodal system is promoted by the short-chain component, which increases the mobility of the system.

Finally, thanks to the activation energy E_d and the free energy barrier ΔG^*, the nucleation rate as a function of temperature can be evaluated with CNT equation (4) (see lines in fig. 5). By using CGMD we can also directly calculate the number of nuclei formed per unit volume and per unit time. For this purpose, we have used a hierarchical clustering method to identify the crystal nuclei and to monitor their size, which we have implemented in a previous work [23].

The nucleation rates directly obtained from our CGMD simulations are shown in fig. 5 (points). We can see that the nucleation rate obtained from the simulations is consistent with that calculated from CNT. According to eq. (4), the temperature dependence of the nucleation rate can be expressed by two exponential factors: the molecular transport term and the energy barrier term. It has been shown [28–30] that these two terms have opposite temperature dependence behavior thereby producing a bell-shaped curve with a maximum rate at the crystallization temperature. The effect of temperature has been widely investigated on the unimodal polymers, whereas rarely mentioned on bimodal polymers. Interestingly, from fig. 5 it can be observed that the nucleation rate of the bimodal system is always larger than that of the unimodal system, indicating that the nucleation rate is promoted by bimodality. The nucleation rate difference of bimodal and unimodal systems mainly stems from the temperature dependence of the size of the critical nuclei, which is eventually a result of chain-folding nucleation of long chain component. Previous works have also suggested an enhanced nucleation rate of bimodal systems. Umemoto *et al.* [30] indicated that the fast nucleation rate of bimodal system is due to intramolecular nucleation mode of long chains in the bimodal system. Song *et al.* [3] found that ultra-high molecular weight polyethylene (UHMWPE) could obviously promote the nucleation rate of high density polyethylene (HDPE), acting as an effective nucleating agent. Kornfield *et al.* [31]. have also shown that the long chains in the blend melt controlled the formation of oriented nuclei.

In conclusion, we have simulated the nucleation of bimodal system and unimodal system with equivalent average molecular weight. A growing probability method has been proposed to calculate the critical size of nucleus over a range of temperatures allowing us to determine the interfacial free energy using a cylinder model and thus the free energy barrier. After obtaining the activation energy of diffusion from the MSD we could then calculate the nucleation rate by applying CNT. The nucleation rate directly calculated from CGMD is qualitatively consistent with the physical expectations stemming from CNT, suggesting that such a simple theory can describe physically complex phenomena. Compared to unimodal polymers, the bimodal system exhibits higher nucleation rate. The simulations and theoretical analysis performed in this work not only reveal the molecular mechanisms of nucleation of bimodal and unimodal polymers, but also generate meaningful methods that can be used for engineering applications.

* * *

All the simulations were performed on the massively parallel computer P2CHPD of FLMSN (Fédération Lyonnaise de Modélisation et Sciences Numériques). The Chinese Scholarship Council is acknowledged for the grant of a doctoral fellowship to ZZ.

Data availability statement: The data that support the findings of this study are available upon reasonable request from the authors.

REFERENCES

[1] Seguela R., *J. Polym Sci. Part B: Polym. Phys.*, **43** (2005) 1729.

[2] Moyassari A., Gkourmpis T., Hedenqvist M. S. and Gedde U. W., *Polymer*, **161** (2019) 139.

[3] Song S. J., Wu P. Y., Ye M. X., Feng J. C. and Yang Y. L., *Polymer*, **49** (2008) 2964.

[4] Wu T., Yu L., Cao Y., Yang F. and Xiang M., *J. Polym. Res.*, **20** (2013) 271.

[5] Jabbari-Farouji S., Rottler J., Lame O., Makke A., Perez M. and Barrat J.-L., *ACS Macro Lett.*, **4** (2015) 147.

[6] Gee R. H., Lacevic N. and Fried L. E., *Nat. Mater.*, **5** (2006) 39.

[7] Uhlmann D. R., Kritchevsky G., Straff R. and Scherer G., *J. Chem. Phys.*, **62** (1975) 4896.

[8] Oliver M. J. and Calvert P. D., *J. Cryst. Growth*, **30** (1975) 343.

[9] Kraack H., Deutsch M. and Sirota E. B., *Macromolecules*, **33** (2000) 6174.

[10] Hoffman J. D., *Polymer*, **33** (1992) 2643.

[11] Hoffman J. D., Miller R. L., Marand H. and Roitman D. B., *Macromolecules*, **25** (1992) 2221.

[12] Milner S. T., *Soft Matter*, **7** (2011) 2909.

[13] Wedekind J., Strey R. and Reguera D., *J. Chem. Phys.*, **126** (2007) 134103.

[14] Yi P., Locker C. R. and Rutledge G. C., *Macromolecules*, **46** (2013) 4723.

[15] Zhang W. and Larson R. G., *Macromolecules*, **51** (2018) 4762.

[16] Zhai Z., Morthomas J., Fusco C., Perez M. and Lame O., *Macromolecules*, **52** (2019) 4196.

[17] Hu Y., Shao Y., Liu Z., He X. and Liu B., *Eur. Polym. J.*, **103** (2018) 312.

[18] Qi S. and Yan D., *J. Chem. Phys.*, **129** (2008) 204902.

[19] Fall W. S., Baschnagel J., Benzerara O., Lhost O. and Meyer H., *ACS Macro Lett.*, **12** (2023) 808.

[20] Achilias D. S., Papageorgiou G. Z. and Karayannidis G. P., *J. Polym. Sci. Part B: Polym. Phys.*, **42** (2004) 3775.

[21] Kampmann R. and Wagner R., *Kinetics of precipitation in metastable binary alloys - theory and application to Cu-1.9 at % Ti and Ni-14 at % Al*, in *Decomposition of Alloys: The Early Stages* (Elsevier) 1984, pp. 91–103.

[22] Zhai Z., Fusco C., Morthomas J., Perez M. and Lame O., *ACS Nano*, **13** (2019) 11310.

[23] Morthomas J., Fusco C., Zhai Z., Lame O. and Perez M., *Phys. Rev. E*, **96** (2017) 52502.

[24] Nébouy M., Morthomas J., Fusco C., Baeza G. P. and Chazeau L., *Macromolecules*, **53** (2020) 3847.

[25] Wu S., *J. Phys. Chem.*, **74** (1970) 632.

[26] Harmandaris V. A., Mavrantzas V. G. and Theodorou D. N., *Macromolecules*, **31** (1998) 7934.

[27] Harmandaris V. A., Mavrantzas V. G., Theodorou D. N., Kröger M., Ramírez J., Öttinger H. C. and Vlassopoulos D., *Macromolecules*, **36** (2003) 1376.

[28] Müller A. J., Michell R. M. and Lorenzo A. T., *Isothermal Crystallization Kinetics of Polymers*, in *Polymer Morphology* (John Wiley & Sons, Ltd.) 2016, p. 181203

[29] Lorenzo A. T. and Müller A. J., *J. Polym. Sci. Part B: Polym. Phys.*, **46** (2008) 1478.

[30] Umemoto S., Hayashi R., Kawano R., Kikutani T. and Okui N., *J. Macromol. Sci. Part B*, **42** (2003) 421.

[31] Kornfield J. A., Kumaraswamy G. and Issaian A. M., *Ind. Eng. Chem. Res.*, **41** (2002) 6383.